Aerial monitoring of atmospheric particulate matter produced by open-pit mining using low-cost airborne sensors

Adrián Zafra-Pérez[1], Carlos Boente[1,2*], Manuel García-Díaz[3], Juan Antonio Gómez-Galán[4], Ana Sánchez de la Campa[1,5], Jesús D. de la Rosa[1,5]

[1]CIQSO-Center for Research in Sustainable Chemistry, Associate Unit CSIC-University of Huelva "Atmospheric Pollution", Campus El Carmen s/n, 21007 Huelva, Spain

[2]Department of Mining, Mechanic, Energetic and Construction Engineering, ETSI, University of Huelva, Huelva, 21007, Spain

[3]Department of Fluid Mechanics, University of Oviedo, C/Wifredo Ricart, Gijón, 33204, Spain

[4]Department of Electronic Engineering, Computers and Automation, University of Huelva, Huelva, 21007, Spain

[5]Department of Earth Sciences, Faculty of Experimental Sciences, University of Huelva, Huelva, 21007, Spain.

[*]*Corresponding author:* carlos.boente@dimme.uhu.es

Abstract

Mining is an economic activity that entails the production and displacement of significant amounts of atmospheric particulate matter (PM) during operations involving intense earthcrushing or earthmoving. As high concentrations of PM may have adverse effects on human health, it is necessary to monitor and control the fugitive emissions of this pollutant. This paper presents an innovative methodology for the online monitoring of PM_{10} concentrations in air using a low-cost sensor (LCS, <300 USD) onboard an unmanned aerial vehicle. After comprehensive calibration, the LCS was horizontally flown over seven different areas of the large Riotinto copper mine (Huelva, Spain) at different heights to study the PM_{10} distribution at different longitudes and altitudes. The flights covered areas of zero activity, intense mining, drilling, ore loading, waste discharge, open stockpiling, and mineral processing. In the zero-activity area, the resuspension of

PM_{10} was very low, with a weak wind speed (3.6 m/s). In the intense-mining area, unhealthy concentrations of PM_{10} (>51 $\mu gPM_{10}/m^3$) could be released, and the PM_{10} can reach surrounding populations through long-distance transport driven by several processes being performed simultaneously. Strong dilution was also observed at high altitudes (> 50 m). Mean concentrations were found to be 22–89 $\mu gPM_{10}/m^3$, with peaks ranging from 86 to 284 $\mu gPM_{10}/m^3$. This study demonstrates the potential applicability of airborne LCSs in the high-resolution online monitoring of PM in mining, thus supporting environmental managers during decision-making against fugitive emissions in a cost-effective manner.

Keywords: Low-cost sensors; PM_{10}; Monitoring; UAV; Mining.

Graphical abstract

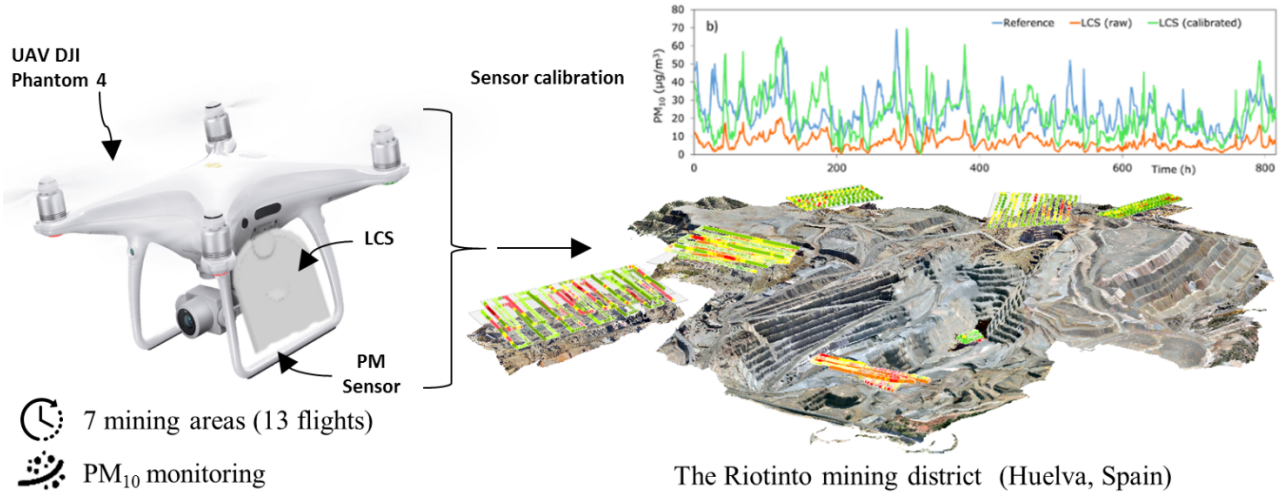

Highlights

- Calibrated low-cost PM sensor was airlifted via unmanned aerial vehicle in a mine.
- Influence of propellers on PM measurements was null at 3 m/s displacement speed.
- Unhealthy concentrations (>51 $\mu gPM_{10}/m^3$) were found near mining operations.
- It has been demonstrated that PM_{10} from the mine reaches nearby towns.
- A strong dilution of PM_{10} with height was observed.

1. Introduction

High concentrations of atmospheric particulate matter (PM) have been associated with many short- and long-term adverse health effects (Kim et al., 2015). The exposure of populations to high concentrations of atmospheric PM has led to an increase in mortality in urban and rural environments in recent years (Mostovenko et al., 2022; So et al., 2022; Liu et al., 2019). Given the evidence regarding the association between PM exposure and daily mortality, the concentrations of atmospheric pollutants are regulated through the Air Quality Guidelines developed by the World Health Organization (WHO, 2021), as well as other similar standards in most countries.

With these established threshold limits for atmospheric pollution, it is essential to develop novel technological methodologies for the accurate quantification of air pollutant transport, as well as introduce them in prevention and Quality Assurance and Quality Control (QA/QC) systems to reduce fugitive emissions, which affect nearby populations (Hassan et al., 2022; Lin et al., 2020). In this context, the use of low-cost sensors (LCS, < 300 USD) for online PM monitoring has gained relevance in recent years (Kang et al., 2022). In contrast to classical fixed-site air quality stations, which are not only immobile but also costly to acquire, operate and maintain (Brauer et al., 2019), properly calibrated LCSs can make near real-time measurements with high spatial and temporal resolution (Snyder et al., 2013). Therefore, LCSs can provide promising results for identifying the spatial trends of PM distribution in air (Giordano et al., 2021; Jovašević-Stojanović et al., 2015). For instance, LCSs have recently been used for online monitoring of PM and air quality mapping in cities by coupling them to cars (Wu et al., 2020), in open-pit mines using pick-up trucks (Zafra-Pérez et al., 2023), or in forests for assessing damage to trees caused by fires (Price and Forehead, 2021).

Existing studies have frequently focused on mapping concentrations at the ground level or at a height of a few metres. However, the concentration decreases with increasing altitude along the vertical axis and with distance from the pollution source along the horizontal axis (Kalaiarasan et al., 2009). In this context, with advances in robotics and electronics, the development of unmanned aerial vehicles (UAV), informally named drones, has eased the acquisition of three-dimensional atmospheric pollution profiles (Dubey et al., 2022a). Thus, sensors coupled to UAV have been

72 used in different applications (Villa et al., 2016a), such as assessments of the vertical distribution
73 of atmospheric pollutants in cities (Rodríguez and López-Darias, 2021; Zhu et al., 2019;
74 Kuuluvainen et al., 2018), and studies of the scattering of PM released during volcanic eruptions
75 (Román et al., 2022; Pering et al., 2020) or ship emissions (Villa et al., 2019). Although a series
76 of technical and procedural considerations must be considered when mounting a sensor on a UAV
77 (Alvarado et al., 2017), these studies have demonstrated the possibility of achieving online PM
78 measurement at various heights.

79 Companies with processes that release large amounts of particulate matter (Liu et al., 2022:
80 Sumadevi et al., 2022; Greguletz et al., 2020) may receive hefty fines or even shut down of
81 facilities for environmental contamination if their control of PM is lacking as it occurred in other
82 mines in the USA (Rodríguez-Chávez et al., 2021; EPA, 2020) or Chile (Castro and Paredes, 2014;
83 Fox, 2023). These policies are not only implemented at ground level but also extended to higher
84 altitudes, aiming to safeguard the well-being of organisms inhabiting various elevations and
85 mitigate potential impacts across atmospheric layers. Therefore, there are lots of stakeholders that
86 are interested in implementing LCS+UAV technologies, such as civil society, monitoring
87 institutions and policymakers.

88 The mining industry is one of the sectors constituting significant sources of PM (Noble et al.,
89 2017), mainly attributable to different operations, such as grinding, mineral processing, open-field
90 storage of size-reduced material, machinery traffic, rock drilling, and blasting (Boente et al., 2022).
91 Accordingly, this study aimed to develop a novel methodology for gaining deeper insight into the
92 spatial distribution of atmospheric aerosols released during mining operations and to assess the
93 degree of dilution of PM_{10} with height and distance in order to evaluate whether mining operations
94 may be hazardous to nearby populations and the environment (Boente et al., 2023). Since there are
95 various physicochemical features of PM_{10}, such as chemical composition, particle size distribution
96 or deposition tendency, influencing its distribution (Zhou et al., 2020). Analysing the vertical
97 dimension alongside the horizontal dimension allows us to evaluate if PM_{10} can ascend to higher
98 altitudes, where wind regimes diverge, potentially leading to greater horizontal dispersion. The
99 study was conducted in the historically prestigious and large Riotinto mining complex (Huelva,
100 SW Spain), more specifically, in the open-pit namely Corta Cerro Colorado, where the Cypriot

company Atalaya Mining owns an operating license that extends up to 2035. The findings of this research are important for providing companies with innovative applications for the aerial monitoring of PM and for determining the contribution of specific mining activities to atmospheric pollution in surrounding areas.

2. Materials and methods

2.1 Study area

The Riotinto copper mining complex is located in the Spanish sector of the Iberian Pyrite Belt. It constitutes one of the largest volcanogenic massive sulfide (VMS) deposits in the world with estimated VMS resources of more than 500 Mt and low-grade mineralisation of approximately 2 Gt (0.41–0.20% in Cu, Atalaya Mining, 2022). The orebody of the VMS in Riotinto mainly comprises pyrite, with minor amounts of sphalerite, galena, chalcopyrite, and traces of grey copper ores and arsenopyrite (De Mello et al., 2022). In fact, the low ore grade coupled with the vast open-pit exploitation, with an extension of approximately 20 km^2, implies massive earthmoving that releases large amounts of PM into the atmosphere. In addition, weather conditions are characterized by low rainfall and dry air with annual mean temperature of 24ºC and relative humidity around 58% (Müller, 2021), which favour the resuspension of dust during periods of strong winds.

Three villages are located next to the mine: La Dehesa, Minas de Riotinto, and Nerva, at distances of 0.2, 1.5, and 4 km, respectively. These three villages sum a total population of 9,000 permanent residents. Thus, in order to keep inhabitants safe, it is important to monitor the PM released by mining activities that may affect them. In this regard, a previous source apportionment revealed that the annual mean contribution of the mine to PM_{10} in these three villages ranged from 2.0 $\mu gPM_{10}/m^3$ to 13.4 $\mu gPM_{10}/m^3$ in 2021 (Boente et al., 2023). In contrast, a study performed when the mine was closed, between 2009 and 2016, stated that the annual mean contribution was 1.0 $\mu gPM_{10}/m^3$ (Sánchez de la Campa et al., 2020). In this regard, the company owning the mine has implemented different abatement systems to avoid fugitive emissions, such as irrigation using

$CaCO_3$-neutralised water from the mining processes. However, previous research has revealed that significant amounts of PM are still released despite the measures adopted (Boente et al., 2022).

2.2 LCS: Technical features, calibration and data validation

Data acquisition for PM_{10} was performed using a consumer-based device and low-cost unit (< 300 USD). Specifically, the unit used was an internal optical particle sensor PMS7003 from Plantower Co. LTD. (Beijing, China), with dimensions of 13.23×9.83×2.79 cm and weight of 42 g introduced inside a plastic shell to avoid damages on the sensor (total weight 170 g) but provisioned with holes to allow entry of PM to the sensor. According to the manufacturer (Yong and Haoxin, 2016), the PMS7003 is a scattered light sensor that uses a fan to attract ambient air to the measuring cavity, where a LED irradiates light induced by a laser in the area of detection. The PM reflects the received light, which is detected by a photodiode detector located at 180º with respect to the LED. The detector then sends electric pulses to a microprocessor which transforms the measurements into mass concentrations of PM_{10}, $PM_{2.5}$ and PM_1, in accordance with the Lorenz-Mie theory (Hagan and Kroll, 2020). The manufacturer declared a high performance of this sensor in PM_{10} measurements, with an effective range of detectable particle concentrations up to 500 $\mu gPM_{10}/m^3$, a maximum consistency error of ± 10% at 100–500 $\mu gPM_{10}/m^3$, a resolution of 1 $\mu gPM_{10}/m^3$, and a durability of more than three years. In this context, previous studies comparing different PM sensors have revealed that Plantower LCSs have an above-average performance, being one of the best among those available in the market (Lambey and Prasad, 2023; Báthory et al., 2022).

The raw PM_{10} data measured by the LCS allows us to distinguish trends, but to provide an accurate result similar to the real concentration value, a comprehensive calibration with regulatory apparatuses is required (Giordano et al., 2021). By default, the specific unit used for this research was calibrated using a normalised aerosol (ISO 12103 – A1) in the desert of Arizona (USA). However, the properties of this material and the climatic conditions in the calibration area are not the same as those in the Riotinto mining complex. Therefore, the Plantower PMS7003 sensor was exhaustively calibrated prior to its use in the sampling campaign. The calibration was performed in accordance with the official European (EU Working Group, 2010) and EPA (EPA, 2021)

156 protocols, and the results were validated through regression methods suggested by Badura et al.
157 (2019).

158 Thus, according to EPA standards (Clements et al., 2022), the calibration involved an outdoor field
159 campaign for 34 days conducted. For this, there were used two apparatuses located in a monitoring
160 station of the Andalusian Air Quality Network (Government of Andalusia, Spain), 75 km south of
161 the study area in the city of Huelva. During this time, simultaneous measurements were taken
162 using the LCS and two equipment:1) A beta attenuation 5014i model (Thermo Scientific, Franklin,
163 USA), with a resolution of 0.1 $\mu gPM_{10}/m^3$, which is a fixed-site monitoring equipment providing
164 real-time and continuous measurements of PM_{10} concentrations with a time resolution of 1 s. 2) A
165 regulatory (UNE-EN 12341, 2015) high-volume air sampler (MCV CAVF-PM1025, 30 m^3h^{-1},
166 Barcelona, Spain) equipped with PM_{10} Munktell quartz fibre filters that collect PM for 24 h. PM_{10}
167 concentrations were determined in the laboratory through a gravimetric standard procedure (UNE-
168 EN 12341, 2015).

169 Once all data for calibration were collected, a temporal resolution transformation was applied by
170 averaging all 1 s measurements from the beta attenuation and LCS for the same 1 h. In this manner,
171 the results between these two devices could be compared (Clements et al., 2022; Zimmerman et
172 al., 2022). Subsequently, a linear regression was performed between a) the MCV and the beta
173 attenuation device, and b) the LCS and the beta attenuation device. Both calibrations serve crucial
174 purposes: the first ensures calibration of PM_{10} for a regulatory apparatus that continuously
175 measures (beta attenuation) using filters every 24 hours (MCV) providing accurate concentration
176 of PM_{10}, while the second calibration aligns a non-regulatory apparatus (LCS) by leveraging the
177 previously calibrated regulatory apparatus (beta attenuation).

178 After confirming adequate quality of the regression, by fulfilling acceptable parameters established
179 in Clements et al., 2022 (also Table 1), we extracted a calibration factor between the beta
180 attenuation device and LCS. This allowed the correction of the raw PM data directly measured by
181 the LCS to transform it into a result similar to that obtained by a regulation device. Another typical
182 correction for the LCS is drift correction, which is related to the loss of precision. This precision
183 degradation arises due to prolonged use over time and exposure to adverse climatic conditions

during the LCS measurements. In this case, it was not necessary because the campaign duration was too short to cause drift effects on the Plantower PMS7003 unit, as stated by Mukherjee et al. (2017). However, authors recommend calibrating the sensor at least once a year (Zafra-Pérez et al., 2023).

Finally, five goodness-of-fit statistical indicators were used to validate whether the corrected LCS PM_{10} concentrations were better proxies for official beta attenuation and closer to the actual values than raw LCS concentrations (Table SM1, Gressent et al., 2020). The indicators were the mean bias (MB), normalised mean bias (NMB), root mean square error (RMSE), normalised mean error (NME), and normalised root mean square error (NRMSE). A further description of these indicators can be found in Supplementary Materials – Part 1.

2.3 UAV

A DJI Phantom 4 quadrocopter (DJI 2016) was used to lift the calibrated LCS. It contains four two-blade propellers 9450S (240 × 127 mm), individually coupled to an electric engine 2312S 800 kV to gain elevation and ensure manoeuvrability. The transmission range of Phantom 4 is 3.5 km when unobstructed and free of interference, which is more than sufficient to cover the expected sampling distance in this study (< 1 km). The weight of the unit was 1380 g, and the battery life was up to 30 min without payload. In this study, a payload of 170 g corresponding to the LCS caused a reduction in endurance of up to 16 min. The UAV is equipped with a digital visual camera of 12.4 megapixels, with a field of view (FOV) of 94º, 20 mm (35 mm format equivalent) f/2.8 focus at ∞. It also has a dual positioning system via GPS and GLONASS, which allows the drone to carry out stable and steady hovering flights to deliver aerial photographs, as well as to determine its position in space and, subsequently, the location of the LCS.

2.4 Sampling campaign: design and implementation (LCS + UAV)

The sampling flights in the mine were conducted by coupling a unit of the LCS with the Plantower PMS7003 sensor to a DJI Phantom 4 UAV. The LCS was fastened to the landing gear of the UAV DJI Phantom 4 using adhesive tape, as shown in Figure 1, while ensuring that the air inlet to the

PM sensor remained open. Other configurations were not possible because of excessive weight and loss of the centre of gravity, which could cause the system to fall during flight.

Given this configuration, the UAV propellers may eject particles arriving at the LCS, thereby affecting the measurements. Villa et al. (2016b) demonstrated that regardless of whether the sensor is attached to the body of a UAV, the measurement is not affected by the propellers. Nevertheless, in this study presenting a novel configuration, an aerodynamic test was performed prior to the flight. The CFD package ANSYS® (ANSYS Inc., 2009) was used to calculate the drone aerodynamics. The 3D model was imported into ANSYS® Design Modeller to create the volume of fluid surrounding the drone. Subsequently, the domain was discretised, resulting in a full tetrahedral mesh of 8M cells. In addition, a sphere of influence refinement around the drone was used to enhance the spatial resolution of the area of interest. This density of cells ensured the accuracy of the results. ANSYS® Fluent software was used to solve the aerodynamics of the model. A k-ε RNG turbulence model was used with a Standard wall function. The boundary conditions are in agreement with those in the literature (Avanzini et al., 2020).

Once the coupling was designed, a series of flights in certain mining areas were proposed. To study the dispersion of PM in the air by the mine, we proposed the following sampling campaign, corresponding to seven areas/mining operations covered by a total of 13 flights at a certain height-metres above the ground where the UAV was launched (Figure 1). The following areas were flown:

- Area 1: Lowest floor of the open pit, or crater. Four flights were conducted at 35, 45, 55, and 65 m above the ground.
- Area 2: Highest floor of open pit 1 flight was performed 40 m above the ground.

Specific mining operations:

- Area 3: Entrance of the open pit: mineral loading through backhoe and intense dumper truck traffic with intense drilling. Two flights at 25 and 30 m above the ground.
- Area 4: Northern spoil heap: during the unloading of coarse waste material. One flight was conducted 25 m above ground level.

- Area 5: Mineral processing area during operation. Two flights were conducted at 40 m and 50 m above the ground.

PM_{10} arrival at surrounding populations:

- Area 6: Open storage of size-reduced material (stockpile) in La Dehesa village located at 200 m. Two flights were conducted at 40 and 50 m above the ground.
- Area 7: Spoil heap of waste material to Nerva village. The flight was performed 12 m above the ground from the launching point at the spoil heap, the minimum height accepted by the UAV, to reach, after a height jump of -40 m, an altitude of 52 m above the ground in Nerva.

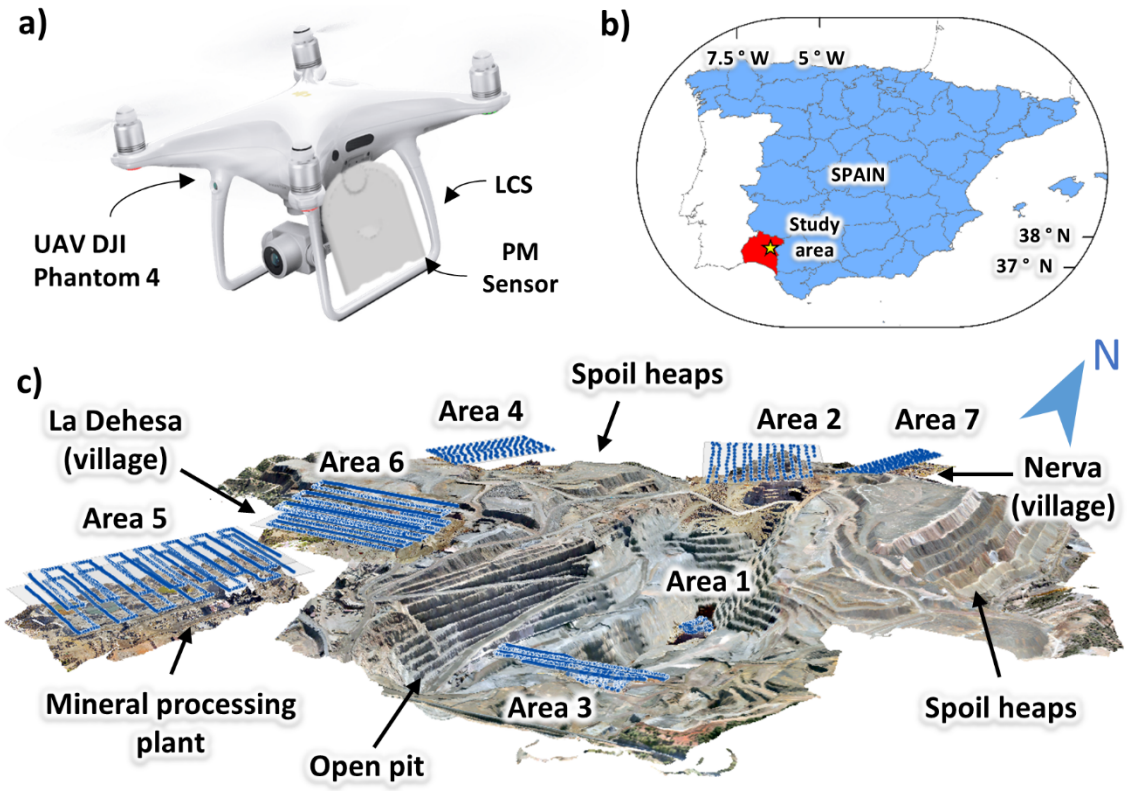

Figure 1. a) Configuration of UAV DJI Phantom 4 and LCS for flight. b) Location of the study area (Riotinto mining complex) in Spain. c) 3D view of the Riotinto mining complex, overflown study areas, main parts of the mine and villages.

All the flights were conducted under the same protocol. They were programmed using the DJI Pilot software for Android OS by adding waypoints along an established route covering the part of the mine to be studied. Each flight consisted of a series of horizontal equidistant transects and was performed at a programmed altitude. This implies that more than one flight would be required to study certain operations at a specific. Based on recommendations of prior authors, it has been opted for a separation of 10 m (Dubey et al. 2022b) or 5 m (Pochwała et al., 2021) for horizontal planes. These distances minimize ambiguities caused by aerosol variations when passing the same location (Villa et al., 2016a). Weather conditions were optimal for the flight and preserving the representativeness of the acquired data: no rain and a low wind speed of < 15 m/s. The duration of each flight is around 15 min, which is the maximum allowed by the battery for this UAV with an additional load of 170 g. Moreover, it was intended to make the wind and flight directions coincide as much as possible in order to assess possible lags in the travel of cloud dusts through wind speed. Take-off, flight, and landing operations were performed autonomously using the programmed UAV (autopilot) with a flight speed of 3 m/s, optimised using ANSYS, to avoid the influence of displacement on the measurements. During flight, the UAV acquires aerial orthophotographs and telemetry logs that provided information on altitude, acceleration, speed, latitude, longitude, pitch, and roll. Simultaneously, the LCS registered data of PM_{10} concentration every second. Smaller sizes ($PM_{2.5}$, PM_1) were not studied because previous research has revealed that aerosols emitted in the study area are mainly composed of coarse particles (PM_{10}, Boente et al., 2022; Sánchez de la Campa et al., 2020).

The operations were carried out following the regulations of the Spanish State Aviation Safety Agency (AESA, 2019), which essentially demands permit acquisition and limits the flight altitude to 120 m above the ground.

2.5 Supporting data and treatment

Additional data were required for the treatment and interpretation of the results. First, hourly wind speed and direction data were obtained from the MeteoBlue© platform. MeteoBlue© is a software that assembles meteorological data from different models (ERA5, NEMS12, NEMS4, NEMSGLOBAL, among others, Müller, 2021), from series ranging from 1984 to the present day

through the premium package History+. The meteorological station selected was Nerva (37.696°N 6.550°W, 336 m.a.s.l.), which is, among those available, the closest to the Riotinto mining complex (3 km). All wind speed and direction data were introduced into the statistical package OpenAir (Carslaw, 2021), which was constructed using the integrated development environment of RStudio (RStudio Team, 2020). The traditional wind rose plot at different intervals was obtained through the "windRose" command of OpenAir in order to study the wind direction and speed during the flights.

Additionally, the topography of the mine during the study period was provided by the mining company and determined by means of a high-resolution Digital Terrain Model (DTM). The DTM was obtained using a Light Detection and Ranging (LiDAR) device, and covered the entire extent of the exploitation (18 km^2). The density of the points was 0.5 points/m^2 and the spatial resolution of the generated DTM was 18 m.

PM_{10} data collected during the flights were geolocated using GPS (x, y, z, coordinates) and loaded into the ESRI ArcScene software (ver 10.8, ESRI 2022) for 3D representation together with the DTM. Moreover, orthophotographs captured by the DJI Phantom 4 were stored in a micro SD card. The photographs were transferred to a computer for processing using Pix4Dreact (ver 1.4.2., Pix4Dreact 2022) to obtain a complete 2D orthomosaic of the flight. The procedure included georectification, filtering algorithms, and the precise reconstruction of the coordinates. Afterwards, the generated orthomosaic was overlapped with the DTM in ArcScene to enable precise detection of PM_{10} sources during the study period. The four data sources (PM_{10}, DTM, orthomosaic, and wind parameters) enabled us to understand the PM_{10} distribution in each situation.

3. Results and discussion

3.1 Evaluation of mobile LCS monitoring in the mining environment

Prior to the realisation of the flights, the calibration of the PM_{10} sensor was assessed to correct the raw data obtained in accordance with the methodology described in Section 2.2, which was previously used by Zafra-Pérez et al. (2023). Figure 2a shows a comparison between the regulatory MCV CAVF-PM1025 large-volume air sampler (MCV) and the 5014i beta attenuation device. Figure 2b shows an intercomparison between the mobile LCS examined and the 5014i beta

attenuation device. The calibrated LCS data (green line) overlapped more with the reference lines (blue) than with the raw data (orange). In particular, the raw data obtained using the LCS were consistently lower than those provided by regulatory apparatuses. This issue was fixed through the calibration. The calibration factor obtained was 3.2.

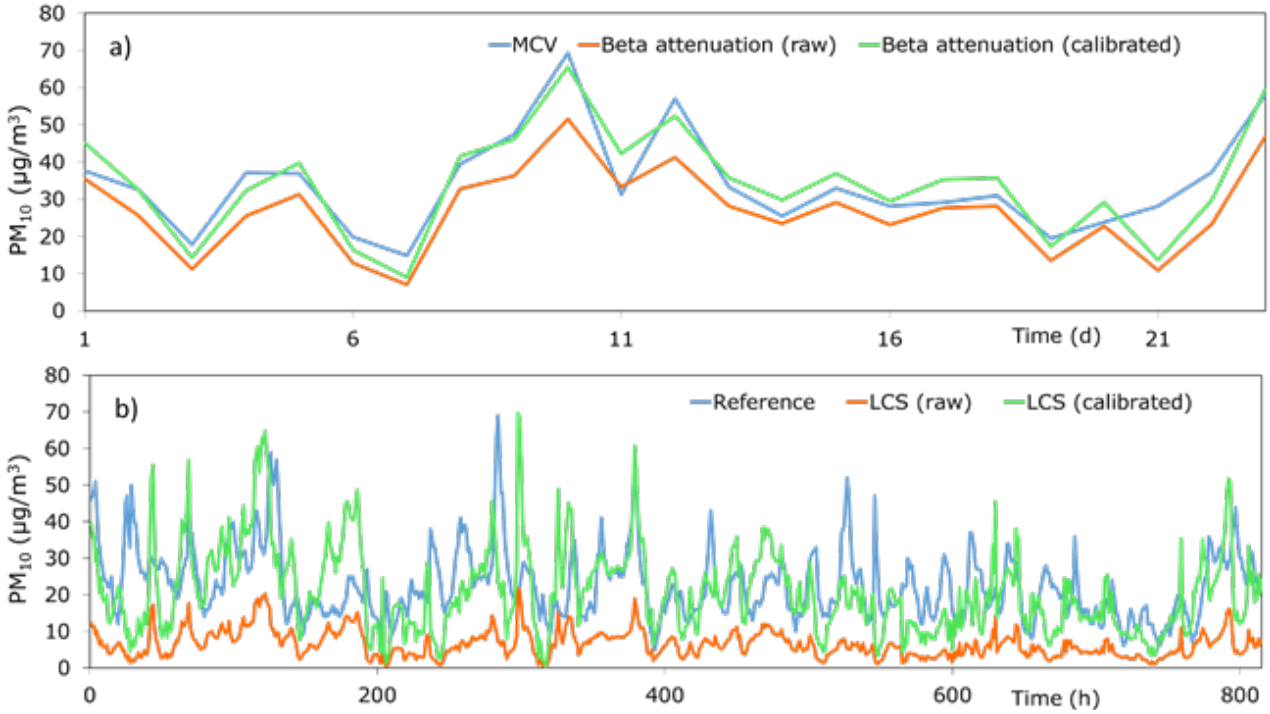

Figure 2. a) Intercomparison between MCV CAVF-PM102 (Reference) and beta attenuation 5014i. Average PM_{10} concentrations for 24 h. b) Intercomparison between mobile LCSs and beta attenuation 5014i (Reference). Average PM_{10} concentrations for 1 h.

Some researchers have stated that these slight differences in the measures performed by LCSs can be attributed to climatic conditions. For instance, Magi et al. (2020) confirmed that high relative humidity can cause the hygroscopic growth of particles, which would introduce errors in measurements. To confirm the reliability of our calibrated data, a comparison with other similar studies using LCSs and reference equipment was conducted, as shown in Table 1. The table also shows the R^2 as well as the goodness-of-fit statistical indicators described in section 2.2.

First, the average concentration of PM_{10} for the calibrated data in the LCS was a better proxy for those of the reference equipment than the raw data, which was expected (Figure 2). The R^2 value

(0.77) was relatively high and the deviations obtained for the goodness-of-fit indicators were lower for the calibrated data. In this context, Gressent et al. (2020) revealed that to ensure a correct measure of the concentrations of PM_{10} by the sensor, the following requirements must be fulfilled with these statistical indicators: $|MB| \leq |NMB| \leq |RMSE| \leq |NME| \leq |NRMSE|$. This requirement was satisfied in our study as $|-1.76| \leq |-7.75| \leq |11.9| \leq |39.9| \leq |52.6|$. Finally, compared with other studies (Huang et al., 2022; Bauerová et al., 2020, Table 1), it can be noted that our deviation parameters present lower values and the regression coefficient is higher. Therefore, it was concluded that the calibration improved the sensor, and the obtained calibrated data would be similar to those obtained using the reference equipment for PM_{10}.

Table 1. Concentration of PM_{10} from raw and calibrated data, results of linear regression between LCS and reference equipment for PM_{10} and deviations for goodness-of-fit statistical indicators described in section 2.2.

Research	**This research**		**Bauerová et al. (2020)**	**Huang et al. (2022)**
LCS used	PMS7003		PMS7003	PMS7003
Calibration method	EPA (Clements et al., 2022)		Not specified, but similar standards to EPA	Not specified, but similar standards to EPA
Reference equipment	Beta attenuation 5014i model		Optical particle analyzer Fidas200	DustTrak DRX Aerosol Monitor 8533
Reference data (µg/m³)	22.6		22.2	7.91
LCS data (µg/m³)	**Raw**	**Calibrated**	**Calibrated**	**Calibrated**
	6.53	20.9	24.3	3.55
Statistical indicators	**Deviations**		**Deviations**	**Deviations**
MB (µg/m³)	−16.1	−1.76	−2.51	2.68
NMB (%)	−71.2	−7.75	-	-
RMSE (µg/m³)	18.3	11.9	15.9	12.9
NME (%)	71.2	39.9	-	-
NRMSE (%)	81.1	52.6	-	-
R^2	0.77	0.77	0.62	0.16

3.2 Influence of displacement during PM measurements

Given the development of a novel methodology, the influence of displacement on PM measurements was also assessed for the UAV+LCS configuration using ANSYS Fluent (Figure 3). The figure shows the velocity field around the drone in its mid-plane as well as two important zones. On the one hand, a zone of high velocities occurs on both sides of the UAV body corresponding to the location of the propellers. Air was ejected vertically at a maximum speed of 8 m/s. On the other hand, a zone of low velocity occurs below the UAV body because the air jets moved by the propellers are swiftly dissipated, leaving a residual velocity zone (< 1.6 m/s). Nevertheless, as the holes of entry for the sensor were located at the bottom face of the LCS, these residual velocities did not affect the measurement. On the horizontal axis, the speed of displacement is constant and very low (3 m/s), favouring the entrance of the PM into the sensor and permanent ventilation of the measuring cavity. In view of these assumptions, it can be concluded that the displacement has practically no effect.

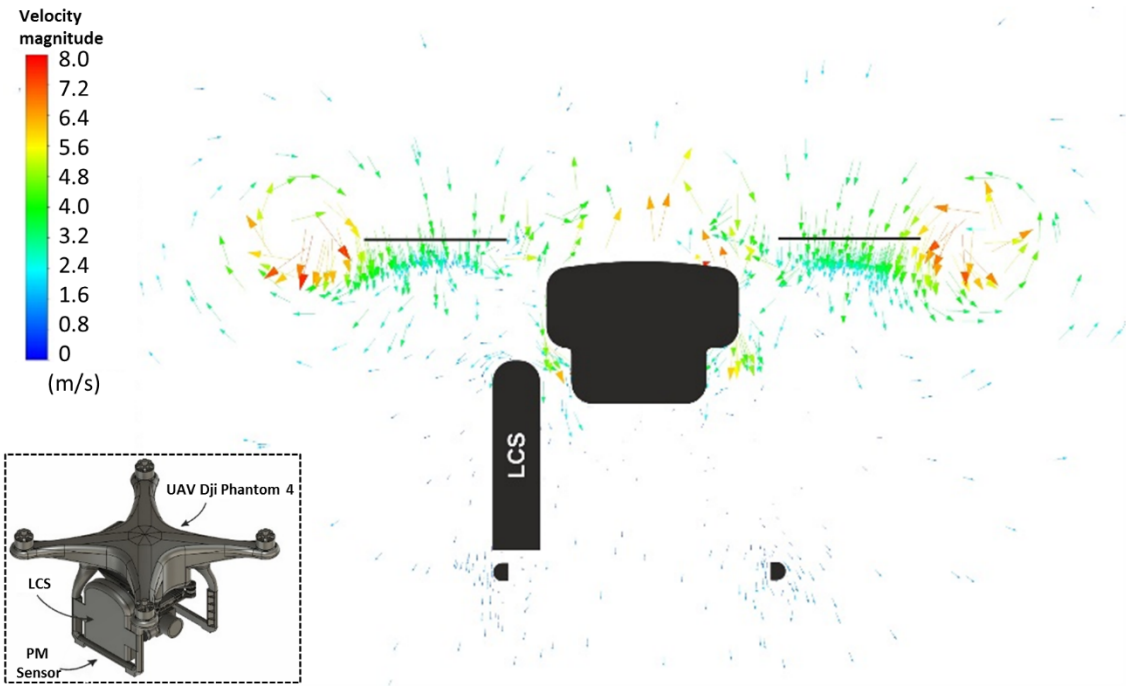

Figure 3. Velocity field around the drone taken from ANSYS Fluent® and 3D model of the UAV along with the LCS.

3.3 PM_{10} levels under the zero mining activity regime

After correcting the raw LCS data through calibration and testing the flight methodology, the results of the different PM_{10} measurements were analysed. To establish comparisons with air quality standards, the ranges of PM_{10} concentrations were categorised according to the categories established by the European Air Quality Index (AQI, European Environmental Agency, 2021). These determine six categories of air quality: good (0–20 $\mu gPM_{10}/m^3$); acceptable (21–40 $\mu gPM_{10}/m^3$); moderate (41–50 $\mu gPM_{10}/m^3$); unhealthy (51–100 $\mu gPM_{10}/m^3$); very unhealthy (101–150 $\mu gPM_{10}/m^3$); hazardous (151–2000 $\mu gPM_{10}/m^3$). It should be noted that AQI is a frequently used indicator by government agencies to assess the air quality in residential or recreational spaces, and our study area was a working environment. However, in this study AQI was used to visualise the data because of the lack of a specific index for working environments.

Figure 4 compares the dust production in the lowest part of the mine with that in the highest part under conditions of low winds (< 3.6 m/s) and without any potential dust producing process in the area. In the lowest part (Figure 4a), the concentrations near the ground (35 m) were mainly at very unhealthy/hazardous levels (> 51 $\mu gPM_{10}/m^3$), but these levels started to decrease with height. Moreover, scattering following the wind direction was also appreciable. This can be explained by the crater accumulating a large amount of dust that is lifted with the winds but up to low heights. Under this scenario, only a small amount of PM_{10} is transported to the upper parts.

The upper part of the mine (Figure 4b) showed a similar pattern. Areas closer to the ground (mainly the left part of the flight and right borders) tended to present more points with concentrations at unhealthy or very unhealthy levels (> 51 $\mu gPM_{10}/m^3$). The centre of the flight, which is more distant from the floor, practically showed no PM_{10} concentrations, but with exceptions related to periodic peaks of air current.

As a conclusion, here we have studied the mine under zero mining activity regime. It resulted that under low wind speed conditions, the crater is not a dust producer. However, the upper part of the mine, being more exposed to adverse weather conditions, can release significant amounts of PM_{10}. In this regard, when the sensor flies close to the ground, PM_{10} levels can reach unhealthy levels, but at a greater distance from the ground, concentrations decrease to acceptable levels.

Consequently, when the mine is not operational, the dust remains localized, and unhealthy levels of PM_{10} do not reach far distances. This finding aligns with previous findings that reported an average of 1.0 $\mu gPM_{10}/m^3$ during mine closure (Sánchez de la Campa et al., 2020).

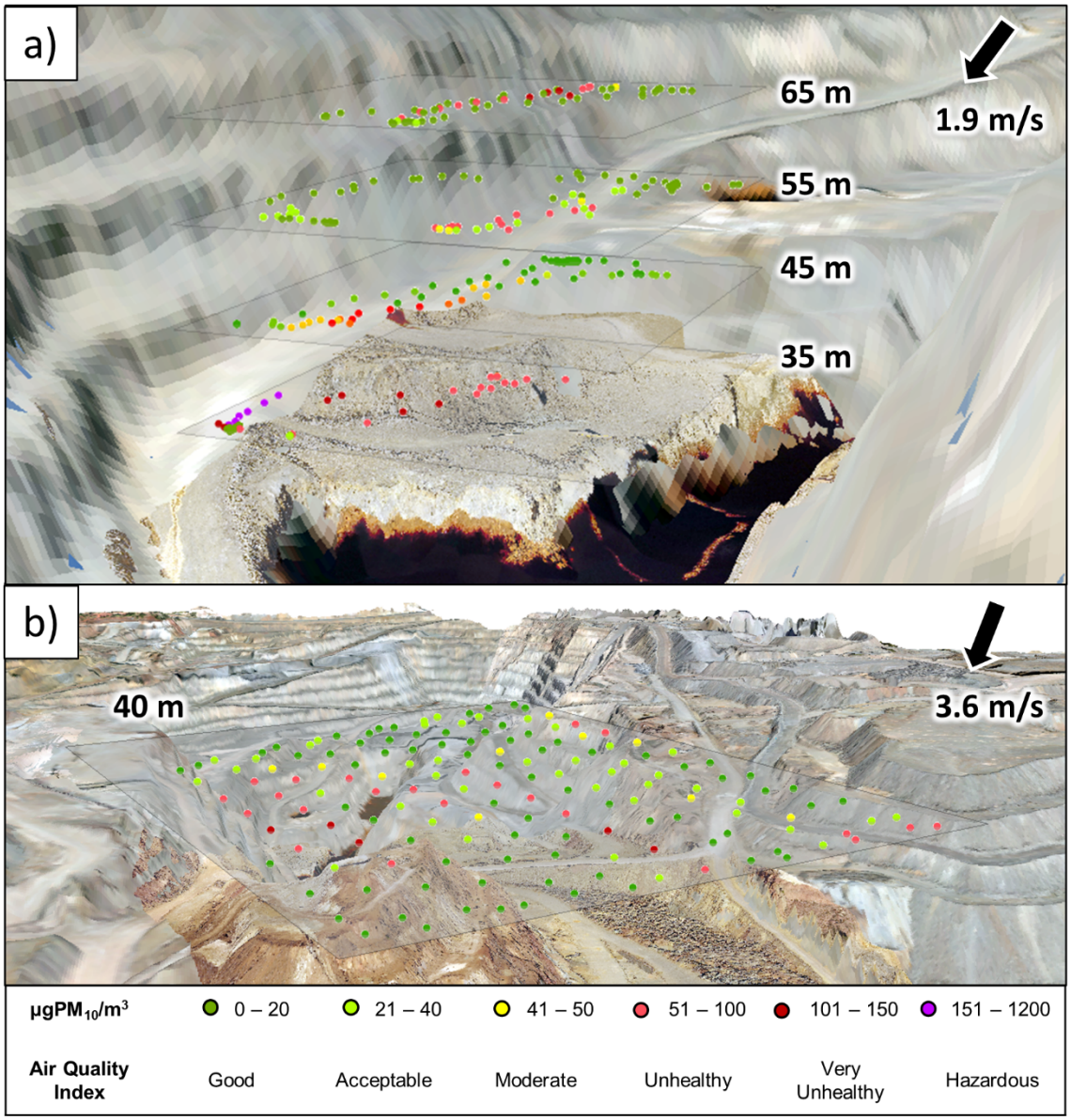

Figure 4. Three-dimensional visualisation of the PM_{10} concentration measurements during horizontal flights at several altitudes for: a) the lowest part of the mine (crater, matches with Area 1 in Figure 1); b) the upper part of the mine (matches with Area 2 in Figure 1).

3.4 PM_{10} levels under the mining activity regime

In addition, the PM_{10} released during specific mining operations was also studied. The area covered in Figure 5a is interesting because multiple mining operations were occurring simultaneously: dry ore loading through the backhoe, drilling, and dumper truck traffic. Under this scenario, the predominant air quality was at a very unhealthy level (> 101 $\mu gPM_{10}/m^3$) in practically the entire area. However, a slight reduction in the PM_{10} gradient with height was observed, represented by an increase in the number of green points, although it was not sufficient to render a global reduction of PM_{10} to acceptable levels. The longest flight (at 25 m height) allowed for the dilution of PM_{10} in an area that was particularly far from the operations and the ground (yellow- green points on the right part of the image).

Figure 5b shows another mining operation—the discharge of waste material. This operation consists of unloading up to 220 t of dry rock from the blasts. In the figure, purple/red points are concentrated in the area above where the dumper trucks unloaded. Moreover, PM scattering occurred along the wind direction. However, in the left part of the figure, the predominance of green points reveals that the dilution of the concentration was very close to that of the dust producer.

In conclusion, typical mining operations such as drilling, ore loading, traffic, and waste discharge lead to the release of atmospheric PM at unhealthy levels. This study revealed that, when considered individually, strong dilution can be observed. However, the accumulation of operations can lead to the formation of unhealthy PM_{10} clouds, for which dilution is difficult and requires greater distances of transport in vertical or horizontal directions. Hence, it is highly advisable to avoid accumulation of mining operations and additionally, to take proactive measures to effectively control dust. Examples include the use of impervious film material on tracks to retain dust through coal/bitumen from polymers or Portland cement (Darling, 2011), or irrigation using $CaCO_3$ neutralised-water, which are methodologies with proven effectiveness in copper mines (Huang et al., 2019). At the Riotinto mining complex, an advanced irrigation system utilizing $CaCO_3$ neutralized-water is employed at regular intervals of 30 minutes. Additionally, in areas characterized by high traffic and intense operational activity, a comprehensive screening process

is implemented using coarse materials sourced from mining spoils. In this context, the technological improvement that constitutes the application of UAV+LCS provides a quicker response to unhealthy concentrations.

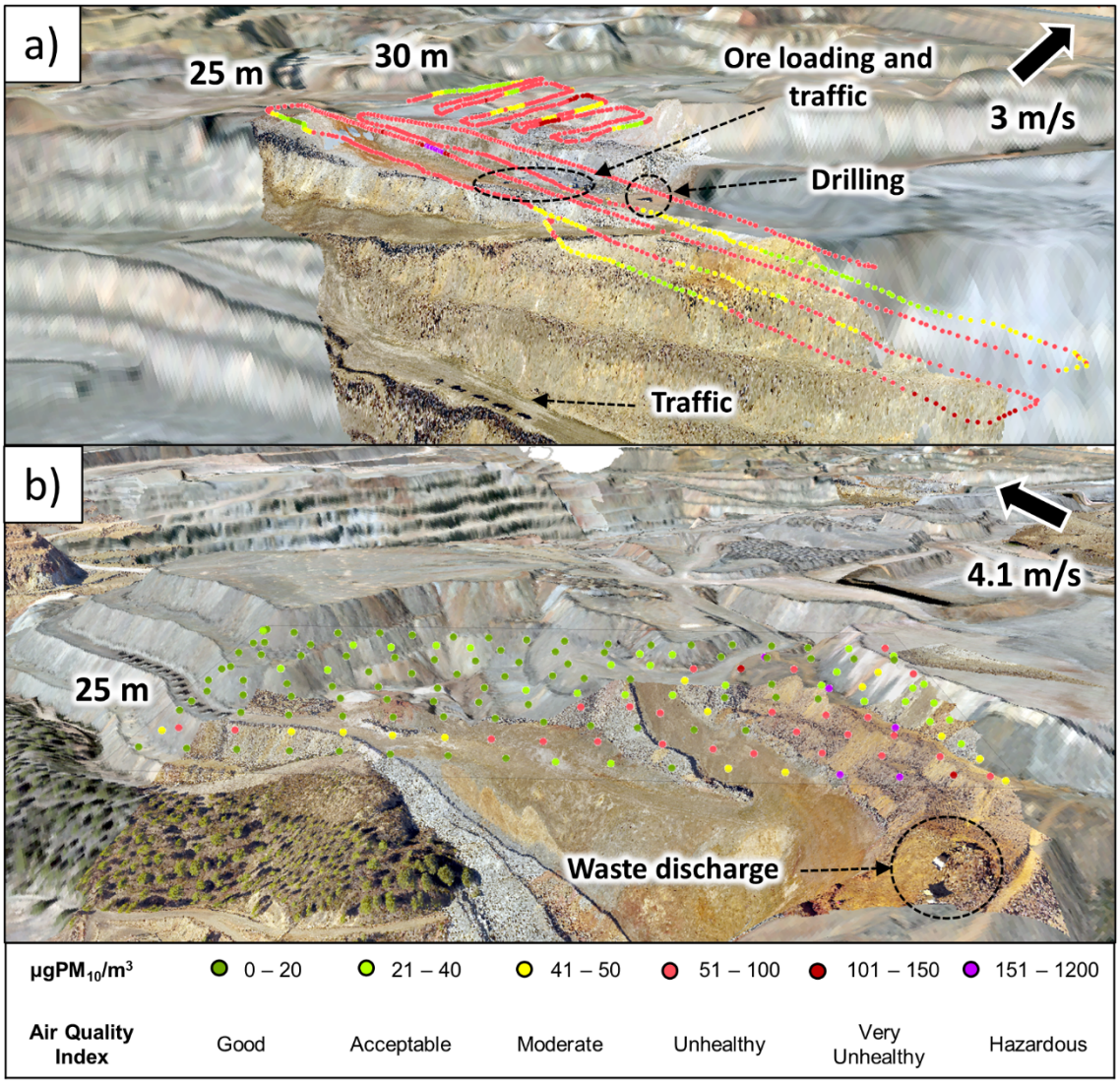

Figure 5. Three-dimensional visualisation of the PM_{10} concentration measurements during horizontal flights at several altitudes for: a) operation of ore loading and traffic (matches with Area 3 in Figure 1); b) operation of waste discharge (matches with Area 4 in Figure 1).

Mineral processing plants are another typical source of PM. Operations such as grinding, milling, and metallic concentration frequently require the movement of size-reduced particles, with the consequent generation of PM_{10} (Boente et al., 2022). Figure 6 shows the mapped results of the

mineral processing plant and the open stockpile of the concentrated product obtained from this plant covered by the LCS flight.

This area presented an alternation of values with high concentrations (unhealthy levels) and others within good or acceptable levels. A dilution with height was not observed, although the high PM_{10} concentrations clearly followed the wind direction, revealing that they came from the mineral processing plant (centre of Figure 6) and the open stockpile (left of the image). In mineral treatment plants, processes are generally performed in closed buildings or equipment. Thus, except for minor leaks during processing or transportation, the release of PM_{10} is not continuous, as it occurs during open-pit operations, such as those explained previously. This explains the periodic nature of the peaks, which mainly occur in air streams. This is also applicable to the stockpile (left of the image). Although it is open, the discharge of the material under wet conditions hinders the release of PM_{10} into the atmosphere.

In general, it can be concluded that PM_{10} fugitive emissions at unhealthy levels can occur and persist at heights up to 50 m according to our results. However, the confinement of operation or the use of water reduces PM emission to the surrounding area, unlike those observed from operations in the open-pit. Moreover, the concerning content of PM_{10} can be attributed to periodic leaks that must be taken into consideration.

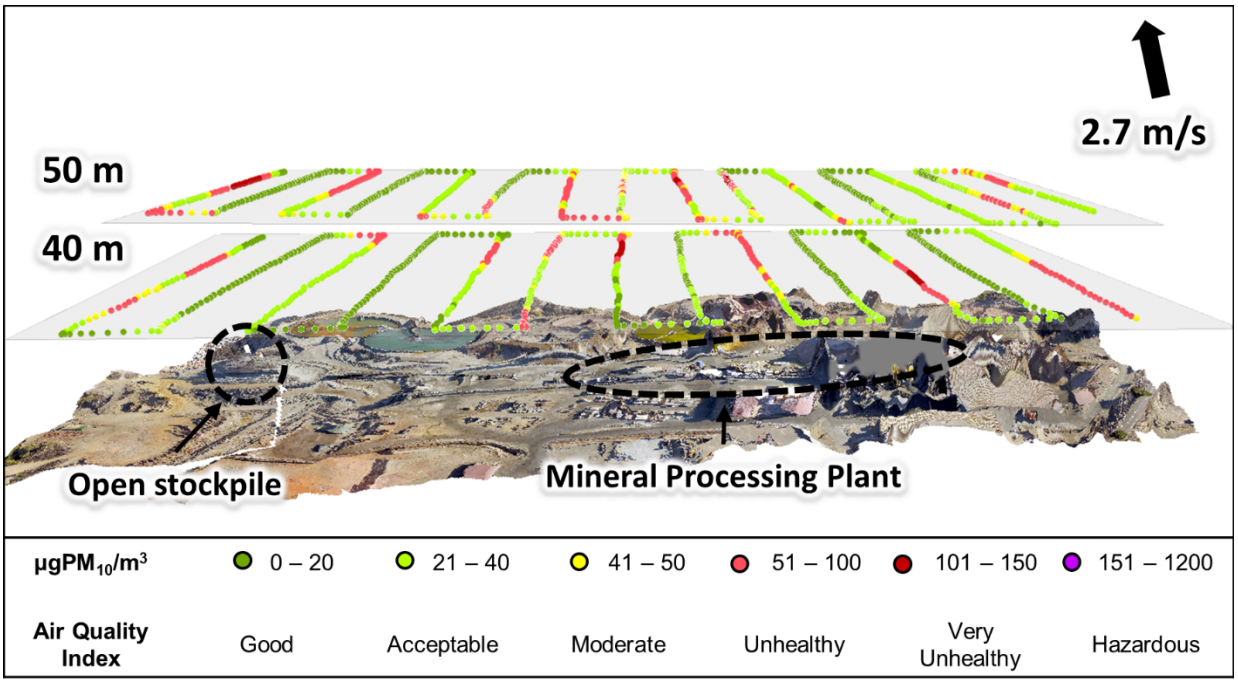

Figure 6. Three-dimensional visualisation of the PM_{10} concentration measurements during horizontal flights at several altitudes for the mineral processing and stockpile areas (matches with Area 5 in Figure 1).

3.5 Effects on surrounding populations

Mining operations have been identified as prominent sources of PM_{10} (Dudka and Adriano, 1997). Airborne LCSs can be further used to assess whether concentrations from the mine can reach surrounding populations. Figure 7 shows two scenarios corresponding to flights from the boundaries of the exploitation area to the nearby villages of Nerva (4 km, Figure 7a) and La Dehesa (0.2 km, Figure 7b). The UAV was flying at the same time as mining activity was happening.

Nerva faces the spoil heap of waste material, an area of the mine that usually presents low activity, except from dumper trucks unloading waste material that, as has been previously discussed, does not represent a concerning operation because the periodic peaks of concentration are rapidly diluted owing to the lack of more sources. As shown in Figure 7a, owing to the large number of green points, the spoil heap does not release concerning amounts of PM when there is no operation, following the patterns previously identified. Moreover, although unhealthy/hazardous points can

be observed in Nerva, a clear discontinuity of concentrations between the spoil heap and the village was observed, which suggests that these extreme concentrations found in the village cannot be attributed to the mine, but to external sources.

La Dehesa village is very close (0.2 km) to a stockpile of fine material and secondary crushing area. Periodic extreme concentrations alternating with low-concentration points were observed, following a pattern similar to that observed in the mineral processing plant area (Figure 6). However, a strong dilution with height was also observed, going from a predominance of unhealthy PM_{10} concentrations at 40 m, to practically presenting good air quality levels at 50 m. This transition of hazardous PM_{10} concentrations from the mining area towards the village, which coincides with the wind direction, must be controlled to avoid potentially hazardous fugitive emissions that present a risk to the population living in this village. In this context, for readers interested in delving deeper into the air quality management and policy implications of the Riotinto mining complex, please refer to the Supplementary Materials – Part 2.

However, it is important to note that these two towns are located at a considerable distance from the mine and are exposed to various sources of pollution. For a more thorough understanding of the mines' contribution to atmospheric pollution in these villages throughout the entire year, we recommend referring to the comprehensive assessment conducted in Boente et al. (2023). The study reveals the presence of multiple sources that contribute to the increase in PM_{10} levels in both villages. These sources can range from natural origins like crustal material or sea salt to anthropogenic factors such as combustion or traffic, albeit in varying proportions. As a result, it can be concluded that the towns may be affected by pollution from multiple sources.

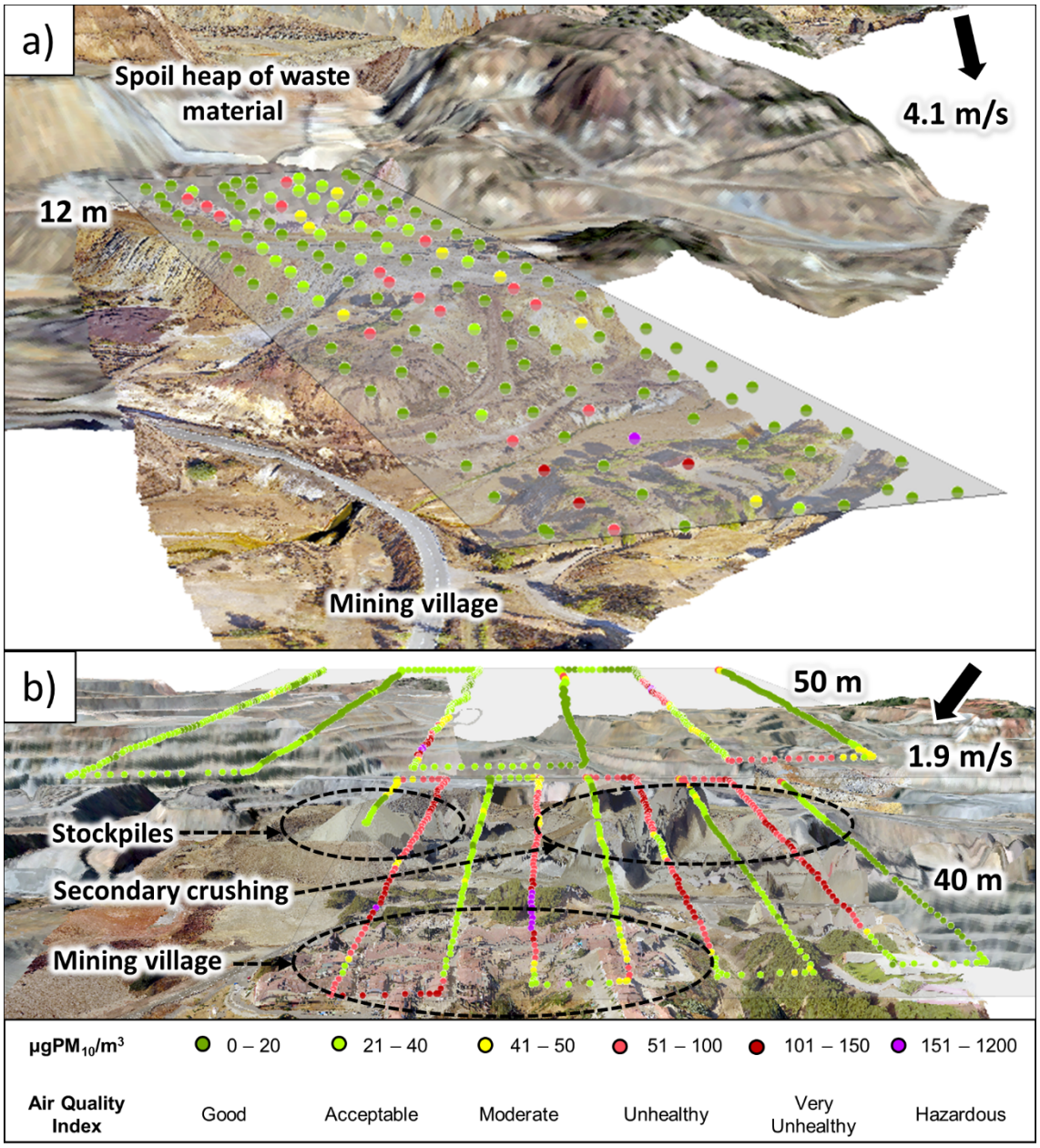

Figure 7. Three-dimensional visualisation of the PM_{10} concentration measurements during horizontal flights at several altitudes in terms of their effects on: a) Nerva (matches with Area 7 in Figure 1); b) La Dehesa (matches with Area 6 in Figure 1).

3.6 Comparison of studied scenarios

A statistical summary of the mining operations considered in this study is presented in Table 2. The percentage of measures (waypoints) were found to be within good or acceptable levels for the majority of the operations studied. Operations and areas presenting more waypoints with unhealthy

485 or higher categories were ore loading, drilling, and traffic (77-82%), the lowest floor of the mine
486 (13-76%), the mineral processing area (21-25%), and the village of La Dehesa (10-42%).

487 PM_{10} concentrations were also found to decrease with height. In this context, the crater, ore loading
488 and traffic, and the village of La Dehesa presented a smaller number of points concerning
489 concentrations (> 51 $\mu gPM_{10}/m^3$) at higher altitudes than at lower altitudes. These findings can
490 also be contrasted using the statistical descriptors. High Relative Standard Deviation (RSD)
491 coefficients imply high data variability. This is consistent with the nature of PM data, which can
492 present extreme and null concentrations over small distances. However, the maximum PM_{10}
493 concentration in the mine was found to be 284 $\mu gPM_{10}/m^3$, and the maximum for all the operations
494 was found to be within 100–200 $\mu gPM_{10}/m^3$. This implies a certain regularity in the PM_{10}
495 maximums that the mine can release, which undergo rapid dilution with height or distance.

496 Finally, three areas presented means that surpassed unhealthy levels. One of them includes two fly
497 heights (30 m – 40 m), corresponding to typical high-PM operations, such as the dry loading of
498 ore, drilling, and traffic, for which dust abatement measures can significantly reduce the amount
499 of PM being lifted. A second, is the village of La Dehesa at a low altitude. Nevertheless, if the
500 flight is limited to the village itself, eliminating the stockpiles belonging to the mine, this mean is
501 reduced to acceptable levels (34 $\mu gPM_{10}/m^3$). The third is the crater at the bottommost height (35
502 m), reaching means of 89 $\mu gPM_{10}/m^3$. However, as we move higher to an elevation of 45 meters
503 and beyond, there is a significant dilution effect resulting in the reduction of PM_{10} levels to an
504 acceptable range of 25-29 $\mu g/m^3$. Finally, it can be concluded that the mine contributes hazardous
505 levels of PM_{10} but they get diluted with height and distance, as it has been evidenced along the
506 research, and the short-term effect of every operation on villages in the surroundings will be low
507 when compared with other activities.

508

509

510

Table 2. Statistical summary of the flights studied. Maximums, means, standard deviations, and relative standard deviations (RSD).

Flights	Height (m)	% of measures per Air Quality Index label ($\mu gPM_{10}/m^3$)						$\mu gPM_{10}/m^3$			%
		Good (0 – 20)	Acceptable (21 – 40)	Moderate (41 – 50)	Unhealthy (51 – 100)	Very Unhealthy (101 – 150)	Hazardous (151 – 1200)	Max	Mean	Std	RSD
Crater (Figure 4a)	35	14%	7%	2%	40%	17%	19%	211	89	60	68
	45	74%	10%	1%	7%	2%	5%	211	28	45	162
	55	62%	21%	3%	13%	0%	0%	86	25	18	74
	65	73%	3%	2%	16%	6%	0%	118	29	33	115
Open-pit upper floor (Figure 4b)	40	46%	27%	9%	15%	3%	0%	132	32	28	86
Ore loading, drilling and traffic (Figure 5a)	30	0%	8%	11%	77%	5%	0%	138	66	19	28
	40	1%	7%	15%	74%	2%	1%	160	63	18	29
Waste discharge (Figure 5b)	25	54%	18%	9%	15%	1%	3%	284	31	42	134
Mineral processing (Figure 6)	40	39%	33%	7%	19%	2%	0%	144	33	24	72
	50	27%	36%	14%	21%	3%	0%	141	37	25	66
Effects on Nerva (Figure 7a)	12	66%	15%	5%	12%	2%	1%	160	22	28	129
Effects on La Dehesa (Figure 7b)	40	15%	33%	10%	26%	14%	2%	179	55	37	67
	50	46%	38%	6%	7%	2%	1%	157	28	25	90

4. Conclusion

In this study, an innovative methodology for assessing PM_{10} concentrations in air using a UAV-borne LCS was developed. First, the LCS was comprehensively calibrated to confirm that the PM_{10} measurements were similar to those obtained using regulatory apparatuses. Subsequently, using the fluid mechanics simulator ANSYS, the propellers of the UAV were confirmed to not have any effect on the measurements when the flight speed is low (3 m/s).

The results revealed that when the mine was not operating, the resuspension of PM_{10} was low at low wind speeds (3.6 m/s). However, mining operations such as traffic, dry ore loading, waste

522 discharge, and drilling or mineral processing can release significant amounts of PM_{10} at unhealthy
523 concentrations (>51 $\mu gPM_{10}/m^3$), which lead to concerning accumulations of PM_{10} that can travel
524 over long distances. Moreover, it has been observed that PM_{10} undergoes significant dilution over
525 short distances when these operations are not conducted simultaneously. Additionally, as altitude
526 increases, there is a general improvement in air quality, with higher altitudes mainly exhibiting
527 better air quality compared to lower ones. Finally, we demonstrated that this methodology
528 facilitates the study of PM_{10} transport from mining areas to surrounding villages. In conclusion,
529 studying different altitudes helps to understand PM_{10} distribution in 3D-space and to assess the
530 impact of winds on its transport. Examining vertical and horizontal axes aids in evaluating dust
531 arrival from the mining complex to nearby towns. Indeed, studying the transport model of PM_{10} in
532 heights is crucial to evaluate whether pollutants can reach neighboring areas or become diluted. It
533 is worth noting that even at high altitudes, dust clouds can lead to atmospheric deposition,
534 influenced by wind speed.

535 Airborne LCSs have proven to be useful tools for the online monitoring of atmospheric particulate
536 matter during specific mining operations. Although their applications remain to be further
537 explored, airborne LCSs have been revealed to be very interesting for mining companies
538 experiencing air pollution problems, as they enable the monitoring of the scattering of the PM
539 produced by mining activities. Thus, by opting for cost-effective solutions, mining corporations
540 can allocate their resources effectively while still obtaining valuable air quality data for their
541 monitoring and modelling needs. Using such results dust abatement or mitigation measures can be
542 applied in certain areas or specific operations, and the contribution of mines to global atmospheric
543 pollution in the surrounding areas can be further investigated.

544 In future studies, it is recommended to employ UAVs equipped with longer-lasting batteries. This
545 enhancement would enable the investigation of the spatial distribution of dust clouds in real-time,
546 to build better 3D modelling of PM_{10} with improved precision in both temporal and spatial
547 dimensions. With them, researchers can gain deeper insights into the dynamics of PM_{10} dispersion,
548 allowing for more accurate assessments of its dilution over time and distance, as well as its
549 implications for human health.

Credit author statement

A. Zafra-Pérez: Writing–Original draft; Investigation; Data curation; Formal analysis; Software; Visualisation. **C. Boente**: Writing–Original draft; Investigation; Conceptualisation; Methodology; Validation; Supervision. **M. García-Díaz**: Data curation; Formal analysis; Software; **J.A. Gómez Galán**: Writing–Review and Editing; Supervision. **A. Sánchez de la Campa**: Writing–Review & Editing; Resources; Supervision. **J.D. de la Rosa**: Writing–Review and Editing; Resources; Conceptualisation; Methodology; Supervision; Funding acquisition; Project administration.

Declaration of competing interest

The authors declare that they have no known competing financial interests or personal relationships that could have appeared to influence the work reported in this study.

Acknowledgements

This research has been performed with funds of the project "*68/83 Contribución de fuentes del material particulado atmosférico en el entorno del distrito minero de Riotinto (2023).*" The authors are grateful to the Atalaya Mining Company for granting permission to carry out this research in their facilities and for their active support.

References

AESA, 2019. Commission Implementing Regulation (EU) 2019/947. http://data.europa.eu/eli/reg_impl/2019/947/2022-04-04 (accessed 12.4.2023)

Alvarado, M., Gonzalez, F., Erskine, P., Cliff, D., Heuff, D., 2017. A Methodology to Monitor Airborne PM_{10} Dust Particles Using a Small Unmanned Aerial Vehicle. Sensors 17, 343. https://doi.org/10.3390/s17020343

ANSYS Inc. ANSYS FLUENT 12.0 theory guide. Chapter 14, ANSYS Inc., Canonsburg, PA, 2009, pp.14–18.

573 Atalaya Mining, 2022. Consolidated and Company financial assessments, pp. 3. https://wp-
574 atalaya-mining-2022.s3.eu-west-2.amazonaws.com/media/2023/03/2023.03.22-ATYM_RNS-
575 2022-Annual-Results.pdf (accessed 12.4.2023)

576 Avanzini, G., Nisio, A. Di, Lanzolla, A.M.., Stigliano, D., 2020. A test-bench for battery-motor-
577 propeller assemblies designed for multirotor vehicles, in: 2020 IEEE 7th International Workshop
578 on Metrology for AeroSpace (MetroAeroSpace). IEEE, pp. 600–605.
579 https://doi.org/10.1109/MetroAeroSpace48742.2020.9160320

580 Badura, M., Batog, P., Drzeniecka-Osiadacz, A., Modzel, P., 2019. Regression methods in the
581 calibration of low-cost sensors for ambient particulate matter measurements. SN Appl. Sci. 1, 622.
582 https://doi.org/10.1007/s42452-019-0630-1

583 Báthory, C., Dobó, Z., Garami, A., Palotás, Á., Tóth, P., 2022. Low-cost monitoring of
584 atmospheric PM—development and testing. J. Environ. Manage. 304, 114158.
585 https://doi.org/10.1016/j.jenvman.2021.114158

586 Bauerová, P., Šindelářová, A., Rychlík, Š., Novák, Z., Keder, J., 2020. Low-Cost Air Quality
587 Sensors: One-Year Field Comparative Measurement of Different Gas Sensors and Particle
588 Counters with Reference Monitors at Tušimice Observatory. Atmosphere (Basel). 11, 492.
589 https://doi.org/10.3390/atmos11050492

590 Boente, C., Millán-Martínez, M., Sánchez de la Campa, A.M., Sánchez-Rodas, D., de la Rosa,
591 J.D., 2022. Physicochemical assessment of atmospheric particulate matter emissions during open-
592 pit mining operations in a massive sulphide ore exploitation. Atmos. Pollut. Res. 13, 101391.
593 https://doi.org/10.1016/j.apr.2022.101391

594 Boente, C., Zafra-Pérez, A., Fernández-Caliani, J.C., Sánchez de la Campa, A., Sánchez-Rodas,
595 D., de la Rosa, J.D., 2023. Source apportionment of potentially toxic PM_{10} near a vast metallic ore
596 mine and health risk assessment for residents exposed. Atmos. Environ. 301, 119696.
597 https://doi.org/10.1016/j.atmosenv.2023.119696

598 Brauer, M., Guttikunda, S.K., K A, N., Dey, S., Tripathi, S.N., Weagle, C., Martin, R. V., 2019.
599 Examination of monitoring approaches for ambient air pollution: A case study for India. Atmos.
600 Environ. 216, 116940. https://doi.org/10.1016/j.atmosenv.2019.116940

601 Carslaw, D., 2021. OpenAir: Tools for the analysis of air pollution data.

602 Castro, R. L., Paredes, P. S., 2014. Empirical observations of dilution in panel caving. Journal of
603 the Southern African Institute of Mining and Metallurgy, 114(6), 455-462.

604 Clements, A., R. Duvall, D. Greene, AND T. Dye., 2022. The Enhanced Air Sensor Guidebook.
605 U.S. Environmental Protection Agency, Washington, DC.
606 https://cfpub.epa.gov/si/si_public_record_report.cfm?Lab=CEMM&dirEntryId=356426
607 (accessed 12.4.2023)

608 Darling, P., 2011. SME Mining Engineering Handbook. Society for Mining, Metallurgy, and
609 Exploration, Englewood, Colo.

610 De Mello, C.B., Tornos, F., Conde, C., Tassinari, C.C.G., Farci, A., Vega, R., 2022. Geology,
611 Geochemistry, and Geochronology of the Giant Riotinto VMS Deposit, Iberian Pyrite Belt, Spain.
612 Econ. Geol. 117, 1149-1171.

613 DJI, 2016. Phantom 4 Specs. https://www.dji.com/es/phantom-4/info#specs (accessed 12.4.2023)

614 Dubey, R., Patra, A.K., Nazneen, 2022a. Vertical profile of particulate matter: A review of
615 techniques and methods. Air Qual. Atmos. Heal. 15, 979–1010. https://doi.org/10.1007/s11869-
616 022-01192-1

617 Dubey, R., Patra, A.K., Joshi, J., Blankenberg, D., Nazneen, 2022b. Evaluation of vertical and
618 horizontal distribution of particulate matter near an urban roadway using an unmanned aerial
619 vehicle. Sci. Total Environ. 836, 155600. https://doi.org/10.1016/j.scitotenv.2022.155600

620 Dudka, S., Adriano, D.C., 1997. Environmental Impacts of Metal Ore Mining and Processing: A
621 Review. J. Environ. Qual. 26, 590–602.
622 https://doi.org/10.2134/jeq1997.00472425002600030003x

623 ESRI, 2022. ArcGIS Desktop: Release 10.2. Redlands, CA: Environmental Systems Research
624 Institute.

625 EU Working Group, 2010. Guide to the demonstration of equivalence of ambient air monitoring
626 methods. https://environment.ec.europa.eu/topics/air/air-quality/assessment_en (accessed
627 12.4.2023)

628 European Environmental Agency, 2021. European Air Quality Index.
629 https://www.eea.europa.eu/themes/air/air-quality-index (accessed 12.4.2023)

630 Environmental Protection Agency, 2021. U.S. EPA. Air monitoring methods - Criteria pollutants.
631 https://www.epa.gov/amtic/air-monitoring-methods-criteria-pollutants (accessed 12.4.2023)

632 Environmental Protection Agency, 2020. U.S. EPA. ASARCO's Arizona Copper Smelter Fined
633 $33,000 for Failing to Comply with EPA Settlement. https://www.epa.gov/newsreleases/asarcos-
634 arizona-copper-smelter-fined-33000-failing-comply-epa-settlement (accessed 14.7.2023)

635 Fox, 2023. Chile shuts down state-owned copper smelter after decades of pollution.
636 https://www.foxnews.com/world/chile-shuts-down-state-owned-copper-smelter-decades-
637 pollution (accessed 14.7.2023)

638 Giordano, M.R., Malings, C., Pandis, S.N., Presto, A.A., McNeill, V.F., Westervelt, D.M.,
639 Beekmann, M., Subramanian, R., 2021. From low-cost sensors to high-quality data: A summary
640 of challenges and best practices for effectively calibrating low-cost particulate matter mass
641 sensors. J. Aerosol Sci. 158, 105833. https://doi.org/10.1016/j.jaerosci.2021.105833

642 Greguletz, R., Andersson, P.U., Cooper, A., Chambers, F., Copley, M.A., Daniels, G., Hamilton,
643 M., Hammond, M., Mohammed, H., Roberts, D.L., Shelton, C., Versteeg, H.K., Mitchell, J.P.,
644 2020. A cross-industry assessment of the flow rate-time profiles of test equipment typically used

for dry-powder inhaler (DPI) testing: Part 1 – compendial apparatuses. Aerosol Sci. Technol. 54, 1424–1447. https://doi.org/10.1080/02786826.2020.1792824

Gressent, A., Malherbe, L., Colette, A., Rollin, H., Scimia, R., 2020. Data fusion for air quality mapping using low-cost sensor observations: Feasibility and added-value. Environ. Int. 143, 105965. https://doi.org/10.1016/j.envint.2020.105965

Hagan, D.H., Kroll, J.H., 2020. Assessing the accuracy of low-cost optical particle sensors using a physics-based approach. Atmos. Meas. Tech. 13, 6343–6355. https://doi.org/10.5194/amt-13-6343-2020

Hassan, H., Kumar, P., Kakosimos, K.E., 2022. The impact of local fugitive particulate matter and emission inventories on air quality and health in dry and arid areas. Sci. Total Environ. 824, 153799. https://doi.org/10.1016/j.scitotenv.2022.153799

Huang, J., Kwan, M.-P., Cai, J., Song, W., Yu, C., Kan, Z., Yim, S.H.-L., 2022. Field Evaluation and Calibration of Low-Cost Air Pollution Sensors for Environmental Exposure Research. Sensors 22, 2381. https://doi.org/10.3390/s22062381

Huang, Z., Zhang, L., Yang, Z., Zhang, J., Gao, Y., Zhang, Y., 2019. Preparation and properties of a rock dust suppressant for a copper mine. Atmos. Pollut. Res. 10, 2010–2017. https://doi.org/10.1016/j.apr.2019.09.008

ISO 12103 – A1, 2016. Fine test dust. Filtration standards & specifications. https://www.iso.org/standard/63386.html

Jovašević-Stojanović, M., Bartonova, A., Topalović, D., Lazović, I., Pokrić, B., Ristovski, Z., 2015. On the use of small and cheaper sensors and devices for indicative citizen-based monitoring of respirable particulate matter. Environ. Pollut. 206, 696–704. https://doi.org/10.1016/j.envpol.2015.08.035

Kalaiarasan, M., Balasubramanian, R., Cheong, K.W.D., Tham, K.W., 2009. Traffic-generated airborne particles in naturally ventilated multi-storey residential buildings of Singapore: Vertical

distribution and potential health risks. Build. Environ. 44, 1493–1500. https://doi.org/10.1016/j.buildenv.2008.07.012

Kang, Y., Aye, L., Ngo, T.D., Zhou, J., 2022. Performance evaluation of low-cost air quality sensors: A review. Sci. Total Environ. 818, 151769. https://doi.org/10.1016/j.scitotenv.2021.151769

Kim, K.-H., Kabir, E., Kabir, S., 2015. A review on the human health impact of airborne particulate matter. Environ. Int. 74, 136–143. https://doi.org/10.1016/j.envint.2014.10.005

Kuuluvainen, H., Poikkimäki, M., Järvinen, A., Kuula, J., Irjala, M., Dal Maso, M., Keskinen, J., Timonen, H., Niemi, J. V., Rönkkö, T., 2018. Vertical profiles of lung deposited surface area concentration of particulate matter measured with a drone in a street canyon. Environ. Pollut. 241, 96–105. https://doi.org/10.1016/j.envpol.2018.04.100

Lambey, V., Prasad, A.D., 2023. Measurement of PM_{10}, $PM_{2.5}$, NO_2, and SO_2 Using Sensors. pp. 89–99. https://doi.org/10.1007/978-3-031-16217-6_6

Lin, Z., Wang, F., Ji, T., Ma, B., Xu, L., Xu, Q., He, K., 2020. Characteristics and the Potential Influence of Fugitive PM_{10} Emissions from Enclosed Storage Yards in Iron and Steel Plant. Atmosphere (Basel). 11, 833. https://doi.org/10.3390/atmos11080833

Liu, A., Yi, J., Ding, X., Deng, J., Wu, D., Huo, Y., Jiang, J., Li, Q., Chen, J., 2022. An online technology for effectively monitoring inorganic condensable particulate matter emitted from industrial plants. J. Hazard. Mater. 428, 128221. https://doi.org/10.1016/j.jhazmat.2022.128221

Liu, C., Chen, R., Sera, F., Vicedo-Cabrera, A.M., Guo, Y., Tong, S., Coelho, M.S.Z.S., Saldiva, P.H.N., Lavigne, E., Matus, P., Valdes Ortega, N., Osorio Garcia, S., Pascal, M., Stafoggia, M., Scortichini, M., Hashizume, M., Honda, Y., Hurtado-Díaz, M., Cruz, J., Nunes, B., Teixeira, J.P., Kim, H., Tobias, A., Íñiguez, C., Forsberg, B., Åström, C., Ragettli, M.S., Guo, Y.-L., Chen, B.-Y., Bell, M.L., Wright, C.Y., Scovronick, N., Garland, R.M., Milojevic, A., Kyselý, J., Urban, A., Orru, H., Indermitte, E., Jaakkola, J.J.K., Ryti, N.R.I., Katsouyanni, K., Analitis, A., Zanobetti,

A., Schwartz, J., Chen, J., Wu, T., Cohen, A., Gasparrini, A., Kan, H., 2019. Ambient Particulate Air Pollution and Daily Mortality in 652 Cities. N. Engl. J. Med. 381, 705–715. https://doi.org/10.1056/NEJMoa1817364

Magi, B.I., Cupini, C., Francis, J., Green, M., Hauser, C., 2020. Evaluation of $PM_{2.5}$ measured in an urban setting using a low-cost optical particle counter and a Federal Equivalent Method Beta Attenuation Monitor. Aerosol Sci. Technol. 54, 147–159. https://doi.org/10.1080/02786826.2019.1619915

Mining Technology, 2018. Ghana fines Newmont, Consar and DRA $2.7m over deaths. https://www.mining-technology.com/news/ghana-fines-newmont-consar-dra-2-7m-deaths/ (accessed 14.7.2023)

Mostovenko, E., Canal, C.G., Cho, M., Sharma, K., Erdely, A., Campen, M.J., Ottens, A.K., 2022. Indirect mediators of systemic health outcomes following nanoparticle inhalation exposure. Pharmacol. Ther. 235, 108120. https://doi.org/10.1016/j.pharmthera.2022.108120

Mukherjee, A., Stanton, L., Graham, A., Roberts, P., 2017. Assessing the Utility of Low-Cost Particulate Matter Sensors over a 12-Week Period in the Cuyama Valley of California. Sensors 17, 1805. https://doi.org/10.3390/s17081805

Müller, M., 2021. Meteoblue: weather close to you. Weather Archive Nerva. Andalusia, Spain, 37.7°N 6.55°W. https://www.meteoblue.com/es/tiempo/archive/windrose/nerva_españa_2513237 (accessed 12.4.2023).

Noble, T.L., Parbhakar-Fox, A., Berry, R.F., Lottermoser, B., 2017. Mineral Dust Emissions at Metalliferous Mine Sites, in: Environmental Indicators in Metal Mining. Springer International Publishing, Cham, pp. 281–306. https://doi.org/10.1007/978-3-319-42731-7_16

Pering, T.D., Liu, E.J., Wood, K., Wilkes, T.C., Aiuppa, A., Tamburello, G., Bitetto, M., Richardson, T., McGonigle, A.J.S., 2020. Combined ground and aerial measurements resolve

719 vent-specific gas fluxes from a multi-vent volcano. Nat. Commun. 11, 3039.
720 https://doi.org/10.1038/s41467-020-16862-w

721 Pix4Dreact, 2022. Release 1.4.2. Photogrammetry software, Prilly, Switzerland.

722 Pochwała, S., Anweiler, S., Deptuła, A., Gardecki, A., Lewandowski, P., Przysiężniuk, D., 2021.
723 Optimization of air pollution measurements with unmanned aerial vehicle low-cost sensor based
724 on an inductive knowledge management method. Optim. Eng. 22, 1783–1805.
725 https://doi.org/10.1007/s11081-021-09668-2

726 Price, O.F., Forehead, H., 2021. Smoke Patterns around Prescribed Fires in Australian Eucalypt
727 Forests, as Measured by Low-Cost Particulate Monitors. Atmosphere (Basel). 12, 1389.
728 https://doi.org/10.3390/atmos12111389

729 Rodríguez-Chávez, T.B., Rine, K.P., Almusawi, R.M., O'Brien-Metzger, R., Ramírez-Andreotta,
730 M., Betterton, E.A., Sáez, A.E., 2021. Outdoor/Indoor Contaminant Transport by Atmospheric
731 Dust and Aerosol at an Active Smelter Site. Water, Air, Soil Pollut. 232, 226.
732 https://doi.org/10.1007/s11270-021-05168-2

733 Román, A., Tovar-Sánchez, A., Roque-Atienza, D., Huertas, I.E., Caballero, I., Fraile-Nuez, E.,
734 Navarro, G., 2022. Unmanned aerial vehicles (UAVs) as a tool for hazard assessment: The 2021
735 eruption of Cumbre Vieja volcano, La Palma Island (Spain). Sci. Total Environ. 843, 157092.
736 https://doi.org/10.1016/j.scitotenv.2022.157092

737 RStudio Team, 2020. R: A Language and Environment for Statistical Computing. R Foundation
738 for Statistical Computing, Vienna, Austria.

739 Sánchez de la Campa, A.M., Sánchez-Rodas, D., Márquez, G., Romero, E., de la Rosa, J.D., 2020.
740 2009–2017 trends of PM10 in the legendary Riotinto mining district of SW Spain. Atmos. Res.
741 238, 104878. https://doi.org/10.1016/j.atmosres.2020.104878

742 Snyder, E.G., Watkins, T.H., Solomon, P.A., Thoma, E.D., Williams, R.W., Hagler, G.S.W.,
743 Shelow, D., Hindin, D.A., Kilaru, V.J., Preuss, P.W., 2013. The Changing Paradigm of Air

744 Pollution Monitoring. Environ. Sci. Technol. 47, 11369–11377.
745 https://doi.org/10.1021/es4022602

746 So, R., Andersen, Z.J., Chen, J., Stafoggia, M., de Hoogh, K., Katsouyanni, K., Vienneau, D.,
747 Rodopoulou, S., Samoli, E., Lim, Y.-H., Jørgensen, J.T., Amini, H., Cole-Hunter, T., Mahmood
748 Taghavi Shahri, S., Maric, M., Bergmann, M., Liu, S., Azam, S., Loft, S., Westendorp, R.G.J.,
749 Mortensen, L.H., Bauwelinck, M., Klompmaker, J.O., Atkinson, R., Janssen, N.A.H., Oftedal, B.,
750 Renzi, M., Forastiere, F., Strak, M., Thygesen, L.C., Brunekreef, B., Hoek, G., Mehta, A.J., 2022.
751 Long-term exposure to air pollution and mortality in a Danish nationwide administrative cohort
752 study: Beyond mortality from cardiopulmonary disease and lung cancer. Environ. Int. 164,
753 107241. https://doi.org/10.1016/j.envint.2022.107241

754 Rodríguez, S., López-Darias, J., 2021. Dust and tropical PMx aerosols in Cape Verde: Sources,
755 vertical distributions and stratified transport from North Africa. Atmos. Res. 263, 105793.
756 https://doi.org/10.1016/j.atmosres.2021.105793

757 Sumadevi, V.K., Anila, U., Roy, K.P., Vishnu, V.B., Minu, S., 2022. Modelling of Air Pollution
758 Dispersion in Thiruvananthapuram Corporation. pp. 341–353. https://doi.org/10.1007/978-981-
759 19-0304-5_25

760 UNE-EN 12341, 2015. Ambient air - Standard gravimetric measurement method for the
761 determination of the PM_{10} or $PM_{2.5}$ mass concentration of suspended particulate matter.

762 Villa, T., Gonzalez, F., Miljievic, B., Ristovski, Z., Morawska, L., 2016a. An Overview of Small
763 Unmanned Aerial Vehicles for Air Quality Measurements: Present Applications and Future
764 Prospectives. Sensors 16, 1072. https://doi.org/10.3390/s16071072

765 Villa, T., Salimi, F., Morton, K., Morawska, L., Gonzalez, F., 2016b. Development and Validation
766 of a UAV Based System for Air Pollution Measurements. Sensors 16, 2202.
767 https://doi.org/10.3390/s16122202

Villa, T.F., Brown, R.A., Jayaratne, E.R., Gonzalez, L.F., Morawska, L., Ristovski, Z.D., 2019. Characterization of the particle emission from a ship operating at sea using an unmanned aerial vehicle. Atmos. Meas. Tech. 12, 691–702. https://doi.org/10.5194/amt-12-691-2019

World Health Organization, 2021. WHO global air quality guidelines: particulate matter ($PM_{2.5}$ and PM_{10}), ozone, nitrogen dioxide, sulfur dioxide and carbon monoxide. https://www.who.int/publications/i/item/9789240034228

Wu, Y., Wang, Y., Wang, L., Song, G., Gao, J., Yu, L., 2020. Application of a taxi-based mobile atmospheric monitoring system in Cangzhou, China. Transp. Res. Part D Transp. Environ. 86, 102449. https://doi.org/10.1016/j.trd.2020.102449

Yong, Z.; Haoxin, Z. Digital Universal Particle Concentration Sensor: PMS7003 Series Data Manual; Plantower: Beijing, China, 2016.

Zafra-Pérez, A., Boente, C., de la Campa, A.S., Gómez-Galán, J.A., de la Rosa, J.D., 2023. A novel application of mobile low-cost sensors for atmospheric particulate matter monitoring in open-pit mines. Environ. Technol. Innov. 29, 102974. https://doi.org/10.1016/j.eti.2022.102974

Zhou, S., Wu, L., Guo, J., Chen, W., Wang, X., Zhao, J., Cheng, Y., Huang, Z., Zhang, J., Sun, Y., Fu, P., Jia, S., Tao, J., Chen, Y., Kuang, J., 2020. Measurement report: Vertical distribution of atmospheric particulate matter within the urban boundary layer in southern China – size-segregated chemical composition and secondary formation through cloud processing and heterogeneous reactions. Atmos. Chem. Phys. 20, 6435–6453. https://doi.org/10.5194/acp-20-6435-2020

Zhu, Y., Wu, Z., Park, Y., Fan, X., Bai, D., Zong, P., Qin, B., Cai, X., Ahn, K.-H., 2019. Measurements of atmospheric aerosol vertical distribution above North China Plain using hexacopter. Sci. Total Environ. 665, 1095–1102. https://doi.org/10.1016/j.scitotenv.2019.02.100

Zimmerman, N., Presto, A.A., Kumar, S.P.N., Gu, J., Hauryliuk, A., Robinson, E.S., Robinson, A.L., 2018. A machine learning calibration model using random forests to improve sensor

793 performance for lower-cost air quality monitoring. Atmos. Meas. Tech. 11, 291–313.
794 https://doi.org/10.5194/amt-11-291-2018